ARCHIVES OF MECHANICS
Arch. Mech. **77** (6), 621–645, 2025, https://doi.org/10.24423/aom.4741

Investigations of column separation influence on pressure waves severity based on results of water hammer experiments in elastically supported pipeline

S. HENCLIK

Hydropower Department, Institute of Fluid Flow Machinery, Polish Academy of Sciences, Gdansk, Poland, e-mail: shen@imp.gda.pl

WATER HAMMER (WH) EVENTS are involved in pipelines when the flow is disturbed by any reason changing its velocity, which produces pressure variations and elastic waves propagating in liquid along a pipeline at the acoustic wave-speed. These phenomena stay more complex if dynamic fluid-structure interaction takes place. More dangerous scenarios may happen in the case of liquid cavitation, which appears when the instantaneous local pressure drops down to the level of the liquid vapor pressure. Bubbles of vapor are created, which can be distributed in specific areas of pipes (distributed cavitation) or may form one larger vapor space between two parts of water column (column separation = CS). In the paper analyses of CS effects are presented based upon experiments performed in the laboratory of the Institute of Fluid-Flow Machinery. Water hammer runs in a copper pipeline fixed to the foundation with elastic supports were generated while pressure oscillations and pipeline vibrations were being measured. For certain initial and boundary conditions CS effects were observed. Analyses of these events were performed for varying initial conditions and support stiffness. The general conclusion is that, more elastic pipeline fixing allows to reduce CS behaviors, more effectively. Further discussion and conclusions are also presented, specifically on WH energy dissipation effects.

Key words: water hammer, column separation, fluid-structure interaction, cavitation, severity index, experimental measurements.

1. Introduction

WATER HAMMER (WH) PHENOMENA use to happen in various scenarios and they may produce significant disturbances in a pipe flow system [1, 2]. They can be involved in pipelines when a steady flow is disturbed (accelerated, slowed down or stopped) and two-way energy transfers from kinetic into elastic potential energy of weakly compressible liquid appear. These behaviors may involve large pressure variations and elastic waves propagating in the liquid along the pipeline at the acoustic wave-speed c. In the simple case of a sudden change in velocity Δv the resulting pressure variation Δp, is determined by a formula known as the

Joukovsky equation, in which ρ is the liquid density:

$$\Delta p = -\rho c \Delta v. \tag{1.1}$$

One can see this is the same dependence as that one between the pressure and velocity at a fluid particle in an acoustic plane wave. This is because WH is an acoustic wave propagating in a specific medium of liquid contained in a pipeline [3]. Therefore, the WH wave-speed c is given with a slightly modified formula, which takes into account the elasticity of pipe walls [1, 4]:

$$c = \left(\frac{K}{\rho}\right)^{1/2} \left(1 + \phi \frac{KD}{Ee}\right)^{-1/2}. \tag{1.2}$$

In the aforementioned equation K is a bulk modulus of the liquid, E is pipe material Young modulus, D and e are, respectively, the diameter of the pipe and thickness of its walls. The coefficient ϕ is usually (for a thin-walled pipe) slightly less than unity and for the current scenario it is assumed as $\phi = 1 - \mu^2$, where μ is the pipe material Poisson ratio [1, 5].

Water hammer events can be especially dangerous in large pipeline installations such as penstocks at hydroelectric power stations where serious accidents were reported in the past and therefore, effective modeling of possible transients is important [5–7]. One of the causes of WH severity are circumferential pipe stresses σ_c, which are the result of pressure increases. For a thin-walled pipe they can be determined as $\sigma_c = pD/2e$, where the ratio D/e for large hydropower penstocks can be greater than 200. Even if no significant damage can happen to the hydraulic system, perturbations in its functioning and other disadvantages may arise during transients because of these stresses, as well as vibration, noise, variation of pressure or cavitation. Therefore, various countermeasures are usually taken in such cases [2, 8, 9]. All these behaviors can be still more complex if the pipeline system is significantly elastic and dynamic fluid-structure interaction (FSI) takes place, as WH energy can then flow between liquid and the structure. WH-FSI phenomena have been of scientific interests for over sixty years and existing models [4, 10–12] have allowed us to explain specific transient behaviors much better than the classic WH theory [1, 2].

Considerations regarding dynamic FSI also produces greater possibilities of energy losses modeling because it can be dissipated in liquid as well as in the structure [13]. In general, the basic type of losses accounted within the WH phenomenon is friction between viscous liquid and the pipe walls. Though many unsteady models of this behavior are developed, proposed and verified [14–17] the quasi–steady one is also frequently used, especially because of its simplicity and the fact that these losses are usually not large and, therefore, not so significant within initial moments of time, when WH loads are the most dangerous. Pipe

wall friction stresses for the quasi-steady model are determined with the following equation:

$$\tau_s = \lambda\rho\frac{(v-w)|v-w|}{8}, \tag{1.3}$$

where w is the velocity of pipe section (thus $v-w$ is a relative liquid velocity) and λ is the resistance factor appearing in the Darcy–Weisbach equation [18]. Local hydraulic friction plays usually a smaller role and pressure losses at certain junctions such as bends, valves or pipe reductions are determined with the local friction factor ζ and a quasi-steady formula $\Delta p = \zeta\rho(v-w)|v-w|/2$. On the other hand, energy can be dissipated in the vibrating structure. The most frequent phenomenon considered by various authors are structural losses in pipe material modeled usually with viscoelastic behavior of the structure [19, 20]. Local structural losses can be also produced in various ways [9, 21–23], however, a significantly important one seems to be energy dissipation at elastic pipeline supports with damping properties [12, 24, 25].

Another important effect within WH events can be cavitation and column separation (CS) behaviors, which are the result of significantly large pressure drops that may happen in hydraulic systems [1, 2, 26–32]. These phenomena may produce various negative effects such as cavitation erosion, increased noise and vibration, lack of hydraulic system efficiency or others [33, 34]. In certain scenarios of CS even the pipe collapse may happen [9, 35]. These effects stay more complex if dynamic FSI is significant, however, there are not too many experimental results of investigations within these problems [4, 36–38]. In the current study the analysis of column separation effects during water hammer events was developed and discussed based on experimental results of transients measured at a pipeline built in the Institute of Fluid Flow Machinery (IMP PAN) laboratory. The pipeline was fixed to the foundation with elastic supports of varying stiffness and water hammer runs were generated for various initial conditions (IC). Due to the pipeline supporting system dynamical FSI played an important role in these experiments. For some of the measured records cavitation and column separation effects were observed. Analyses of these events, specifically towards their severity and its reduction rate, are developed in the paper, using various methods and conclusions are formulated.

2. Water hammer models and basic behaviors

2.1. Water hammer with fluid structure interaction

The classic WH theory is modeled for a straight pipe reach with two hyperbolic partial differential equations (PDEs) of the first order that describe

the liquid flow – continuity and momentum. If dynamic FSI is accounted, the basic, one-dimensional (1D) model is governed by four PDE and, therefore, it is usually referred to as the four equation (4E) model of WH-FSI. Beside two equations for the liquid, another two ones govern the pipe motion [4, 12]. The equations for liquid flow are as follows:

$$\frac{\partial v}{\partial t}+\frac{1}{\rho}\frac{\partial p}{\partial x}=-g\sin\alpha-\frac{4\tau_s}{\rho D},\qquad \frac{\partial v}{\partial x}+\frac{1}{\rho c^2}\frac{\partial p}{\partial t}=2\mu\frac{\partial w}{\partial x}. \tag{2.1}$$

The pipe movement is governed by:

$$\frac{\partial w}{\partial t}-\frac{1}{\rho_s}\frac{\partial \sigma}{\partial x}=-g\sin\alpha+\frac{\tau_s}{e\rho_s},\qquad \frac{\partial w}{\partial x}-\frac{1}{\rho_s c_s^2}\frac{\partial \sigma}{\partial t}=-\frac{\mu D}{2Ee}\frac{\partial p}{\partial t}. \tag{2.2}$$

In these equations x and t are standard independent variables of position measured along the pipe and time, ρ_s is a density of pipe material, σ are longitudinal pipe stresses and c_s is velocity of longitudinal elastic waves in pipe walls ($c_s^2 = E/\rho_s$). One can see, that both groups of equations are coupled due to friction terms proportional to τ_s and dependent on both velocities v and w as it is stated in Eq. (1.3). The second coupling mechanism is the Poisson effect which is produced by terms proportional to the Poison ratio μ. These couplings are more clearly visible after a specific transformation of the governing equations, which also allows us easily to draw conclusions about their general solutions [12]. They are two coupled waves – a WH and a structural one (it is also known as precursor because of the higher propagation wave-speed). The coupling between these waves can be noticed at pressure records where oscillations of higher frequency can be observed as superimposed on the main WH wave. A complex pipeline is modeled as a collection of several straight pipes connected at junctions where proper boundary conditions (BC) should be defined. Movable junctions are an important FSI factor as they may produce the third coupling mechanism between fluid and the structure known as junction coupling. A specific BC important also for energy dissipation effects is valid at a node where the pipeline is fixed to the foundation with a viscoelastic support. The boundary condition in such a case can be formulated with an adequate differential equation of junction motion solved numerically concurrently with the main governing equations. This way it can be simulated how the energy is dissipated due to this effect [12].

The basic 4E model is relatively simple, however, it is quite effective and frequently used. Much more complex is the standard model which consists of fourteen equations – additional two for the pipe torsional motion and twice by four equations for lateral movement of the pipe in two perpendicular planes (pipe with water is modeled as a Timoshenko beam) [4, 10]. If viscoelastic effects are to be considered, additional terms are introduced into the governing equations.

2.2. Cavitation and column separation

In specific WH scenarios more complex behaviors may appear when the pressure drops significantly to the level of the vapor pressure of the liquid. Bubbles of vapor are created then, which can be distributed within a certain liquid volume or collected in a larger space forming one bigger vapor cavity separating two columns of water. The former type of two phase flow is known as distributed cavitation, the latter phenomenon – column separation (CS) effect and it may also appear at pipeline ends. For a temperature of 20 °C the saturated vapor pressure of water is $p_v = 2.34\,\mathrm{kPa}$, so it is quite small (about 2% of 1 atm). Another type is gaseous cavitation which may also happen at a certain low pressure, when gasses dissolved in water are released. However, this effect is usually of less importance for our analyses, mainly because it is a much slower process and can be minimized by reducing the amount of free gasses.

Cavitation is known to produce various disadvantages for hydraulic systems such as vibration and noise, cavitation erosion, lack of hydraulic system efficiency, etc. Distributed cavitation results also in changes of the elastic wave propagation velocity in such a liquid-gas mixture. Still more complex behaviors may appear when CS events are involved. One of the most dangerous one is the pipe collapse caused by atmospheric overpressure. It may seem slightly unexpected as pipes are usually resistant to high inside pressures however, outside overpressure may lead to a loss of pipe stability and its destruction as a result of collapse can be much easier. This problem can be analyzed within different aspects [35] and one of typical results of stability loss of a thin-walled, long, circular tube due to uniform outside overpressure can be found in the following form [39]:

$$p_{\mathrm{crit}} = \frac{2E}{1-\mu^2}\left(\frac{e}{D}\right)^3. \tag{2.3}$$

One can calculate, that for a steel pipeline and outside pressure of 1 atm with vapor pressure p_v inside, the stability is lost at $D/e = 166$, which is not such a big value if we consider geometries of large penstocks. Obviously, such pipelines have usually additional reinforcements formed as special ribbings fixed tightly around it and repeated equally at adequate separations. Besides, dedicated procedures for safe exploitation of such structures are usually applied. However, one can see that unexpected CS events can be dangerous. Another effect involved by CS happens when the vapor cavities are collapsed. Secondary WH actions of very steep (and possibly larger) pressure jumps are generated then due to collisions of two water columns during collapse [27, 29, 40]. These effects may also involve additional noise and vibration especially if dynamic FSI is significant.

A simplified model of the WH cycle and CS creation is illustrated in Fig. 1 where it is presented based on the assumptions of no pipe wall friction and no

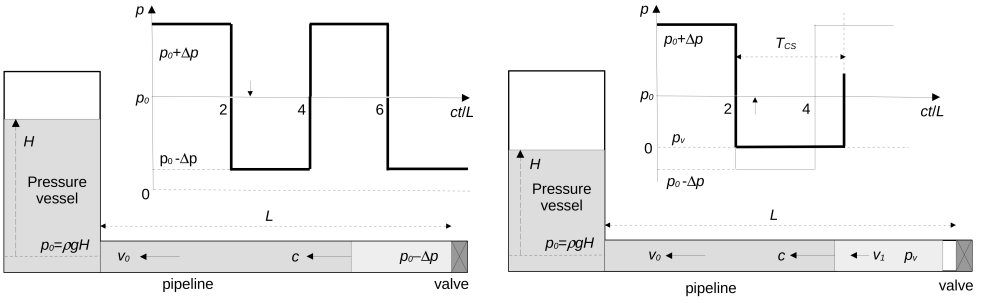

FIG. 1. A scheme of WH wave propagation and pressure records near the valve for a case with and without column separation: (a) decompression at the third quarter of WH cycle; (b) the same phase for column separation conditions, $p_0 < \Delta p$.

dynamic FSI (the pipe is quasi-rigid). In such a case after sudden closure of the valve during a steady flow of velocity v_0 driven by a constant pressure p_0 produced by the vessel, the WH phenomenon is excited. The pressure run at the valve versus time forms a rectangular record of an amplitude given with formula (1.1) oscillating around the static value p_0. A front of the compression pressure wave is traveling towards the vessel at the first quarter of the cycle, then it reflects and travels back. At the third (Fig. 1(a)) and fourth quarters the scenario is repeated, but with the decompression wave. Finally, the pressure oscillates with frequency $f_{\mathrm{WH}} = c/4L$ which is the basic WH frequency $f_{\mathrm{WH}} = f_0$, while all the harmonic components have their frequencies being odd multiplies of this basic one [23]. However, this behavior is different if the value of the Joukovsky pressure drop Δp, given with Eq. (1.1) is larger than the static pressure p_0. Then, at the third quarter of the cycle presented in Fig. 1(b) it cannot drop to the value $p_0 - \Delta p$ because it is negative. So it drops to zero or in fact to the level near the saturated vapor pressure p_v and this drop is not Δp, but $\Delta p_1 = p_0 - p_v$. Therefore, the backward liquid flow is not stopped but only reduced to the value v_1 which can be estimated with the following relation [27]:

$$v_1 = v_0 - \Delta v_1, \qquad \text{where} \qquad \Delta v_1 = \frac{\Delta p_1}{\rho c} = \frac{p_0 - p_v}{\rho c}. \tag{2.4}$$

In such a case the liquid detaches from the valve, a cavity is formed near it and begins to grow, becoming larger and allowing to be filled with vapor. This cavity exists for a time longer than $2L/c$ required for the compression wave to be back.

2.3. Column separation severity estimation

A thorough historical overview of research as well as explanations and discussion on column separation phenomenon during water hammer can be found

in [27]. It is also discussed in classical textbooks on water hammer [1]. Basic modeling method (Discrete Vapor Cavity Model = DVCM) is based on the assumption that at certain sections, where pressure drops to the vapor one, there is a fixed condition of constant pressure and the size of the bubble is calculated according to the inflow and outflow to this section. If finally, the cavity disappears the pressure rise is given with the Joukovsky equation (1.1) according to relative velocities of adjoining water columns. Particular implementations of DVCM, as well as other models are developed and proposed by various scientists [27, 28, 41, 42], however, they are not discussed in this study.

In many applications the time duration of the first vapor cavity can be used as a measure of CS severity estimation. The analysis of this parameter for a simple model of WH with CS has allowed us to propose the following approximate formula for this time T_{cs1} [1, 27]:

$$T_{\mathrm{cs1}} = \frac{\Delta p}{\Delta p_1}\,\frac{2L}{c}. \tag{2.5}$$

Thus, it can be estimated that for $p_v \ll p_0$ this time is $T_{\mathrm{cs1}} \simeq 2L\rho v_0/p_0$. In fact, for various complex cases of pipe flow hydraulic systems this time can be slightly different, which may be dependent on various factors. In the current study we assume the true time duration T_{cs} can be expressed in relation to the theoretical value proposed above. Currently, the reason of some bias between the true and theoretical duration times can be FSI effects in a pipeline fixed with elastic supports. Therefore, we express the true duration time T_{cs} in the following way:

$$T_{\mathrm{cs}} = \beta T_{\mathrm{cs1}}. \tag{2.6}$$

Values of the parameter β for the current experimental results are determined and discussed in the following sections. On the basis of the first vapor cavity duration time, Martin proposed [27, 43] the cavitation severity index S, to be defined by a comparison of this time to $2L/c$, which is doubled time of traveling the wave along the pipeline:

$$S = \frac{T_{\mathrm{cs}}}{2L/c}. \tag{2.7}$$

We can see, if $T_{\mathrm{cs}} = T_{\mathrm{cs1}}$ then $S = \Delta p/\Delta p_1$. In fact, this value can be assumed as a theoretical severity index $\tilde{S}$:

$$\tilde{S} = \frac{\Delta p}{\Delta p_1}. \tag{2.8}$$

Other authors proposed also somewhat different severity indexes however, in this paper we use that one given with Eq. (2.7). Its comparison with the theoretical

value $\tilde{S}$ is also exploited. The CS phenomenon can be also characterized by other specific features. One of them are secondary WH pulses involved when water columns are joined while the vapor cavity collapses. This effect produces a very steep pressure jump. In specific conditions its theoretical height can be even larger than the initial Joukovsky pulse [1, 27, 28, 32]. However, in real systems, when various dissipation effects happen, the subsequent pressure amplitudes get lower. This is the result of various factors and some of them are specific to CS behaviors, which can be associated with irreversible thermodynamic phase transitions or increased friction of complex origin [29, 40, 42, 44]. Besides, energy is also dissipated due to the increased level of generated noise and vibrations, which is particularly important in the case of strong FSI.

3. Experimental measurements

3.1. Laboratory pipeline

The experimental pipeline, fixed to the foundation with various types of elastic supports, was designed and built in the IMP PAN laboratory and dedicated to investigations of FSI influence on water hammer. In fact, WH runs without CS effects were mostly of importance however, additional experiments with CS effects were also performed. Various variables describing the motion and behavior of the system were acquired. Currently pressures measured at four positions along the pipeline and vibrations at three places are of the main interest. For pressure measurements Keller PA-25 transducers were used. A partial view and a general scheme of the test rig are presented in Fig. 2. A copper, mea-

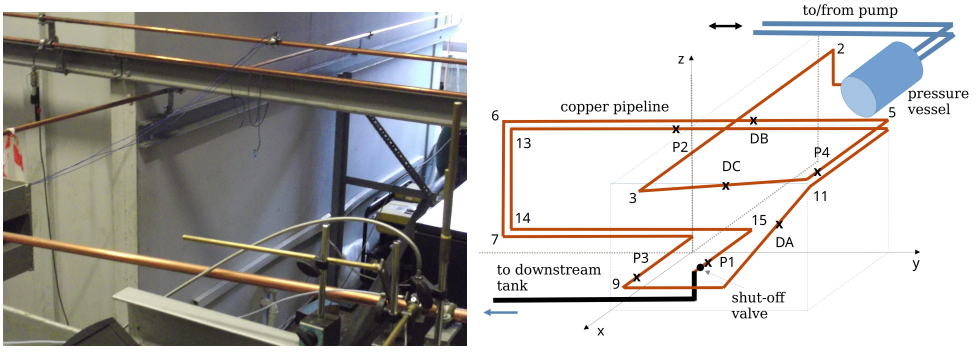

(a) (b)

Fig. 2. A view of the copper pipeline (a) and a general scheme of the test bench with the measurement pipeline (b) [13]. Selected transducers are marked as: DA, DB – accelerometers; DC – displacement sensors; P1, P2, P3, P4 – pressure gauges.

surement pipeline of a total length of $L = 58.7$ m, inner diameter $D = 20$ mm and pipe-wall thickness $e = 1$ mm consisted of several straight pipe reaches joined with knees. It was fixed to the foundation with $N = 25$ elastic supports and two rigid mountings at both pipeline ends. Four types of elastic supports FS2, FS3, FS4, FSR, which are presented in Fig. 3, made as steel flat springs, were used in measurements. Their flexibility coefficients in the vertical direction were determined to be: 2.1 mm/N (FS2), 0.34 mm/N (FS3), 0.085 mm/N (FS4) and 0.88 mm/kN (FSR) [11]. Extended investigations with different methods have allowed us to find slightly different values for some of these parameters [mm/N]: 2.0 for FS2, 0.35 for FS3, 0.088 for FS4. This information allows the reader to judge the rigidity of the whole system because for a detailed modeling the overall stiffness (flexibility) matrix of all supports should be required. This problem is discussed in a more detailed way in [45]. Due to the currently analyzed configuration of supports, mounting systems with their various types are denoted as L2, L3, L4 and LR. The general description, range of measurements and tests performed are included in the previous paper [11] and also in internal reports of the IMP PAN (not published), where the detailed geometry and description of the pipeline is presented. The most important, general information is also specified in this document. Elastic supports were situated close to each bend except for #1 and #15 ones, where no supports were provided. At bend #2 support FSR was used permanently, the others 24 were exchanged. They were spaced along the pipeline with similar separations between neighboring supports equal usually of about 2.4 m. The longest pipe reach of the length about 9.9 m was between bends #5 and #6. Two pipe reaches were neither horizontal nor vertical. Inclination versus horizon of the pipe reach between bends #3 and #4 was 4.4° and between bends #10 and #11, it was 45.4°. In experiments ordinary tap water was used, however, it was deaerated by leaving it calm for at least two days in the downstream reservoir after filling.

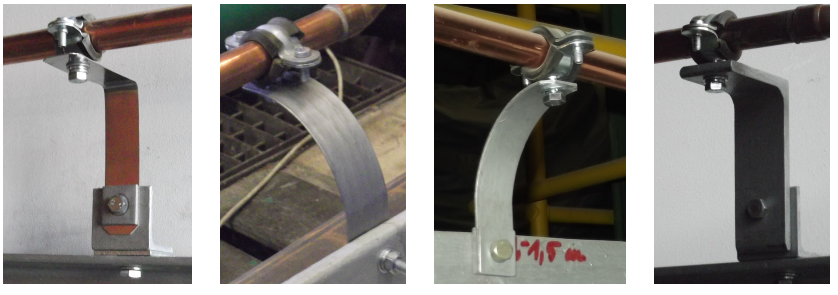

(a) FS2 (b) FS3 (c) FS4 (d) FSR

FIG. 3. Steel flat springs used for supporting the pipeline [11, 13, 45].

The initial steady flow of velocity v_0 was driven by the pressure vessel of constant pressure p_0. WH events were excited by fast (within 5 msec) closure of the shut-off valve (see Fig. 2(b)) driven by a special mechanism. A photo of the main valve, its driving mechanism as well as the pressure acquisition system with an elastic hose from the pipe to the pressure gauge are presented in Fig. 4. The transducer (P1) is fixed to the foundation with elastic arrangement to protect it from vibration of the structure. It is not visible here, however, another pressure gauge (P2) can be barely noticed at the picture (the left upper corner) in Fig. 2(a). When longer closure times were required they were executed just by a hand (a handle was used instead of driving mechanism). Therefore, they were not perfectly repeatable, however, their closing times were longer, equal approximately to 35 ms (±5 ms). The initial flow velocity was measured with ultrasonic flow meter and also controlled by the volumetric flow meter presented in Fig. 4. Various physical variables describing the system motion were measured and digitally acquired. Firstly, the results were acquired within a frequency band up to 5 kHz sampled with 10 kHz. However, finally they were usually analyzed in a resampled form, digitally filtered down to a band up to 1 kHz and sampled with 2 kHz. In this study pressures and vibration are of interest, thus positions of these transducers are revealed in Fig. 2 and presented in Table 1. They are expressed in a relative form as x/L, where x [m] is a true position measured from the pipeline beginning ($x = 0$ at the vessel). Vibrations were measured with accelerometers at DA (B&K 4371) and DB (PCB 357B03) or eddy current displacement sensors type MDS10/MDT10 at DC. The nodes with accelerometers were situated in the middle between two neighboring supports and DC node was close to a support. At each node three coordinates of vibrations were measured, $0x$ – along the current pipe, $0y$ – along a horizontal axis perpendicular to it and $0z$ – along an axis lying at the vertical plane.

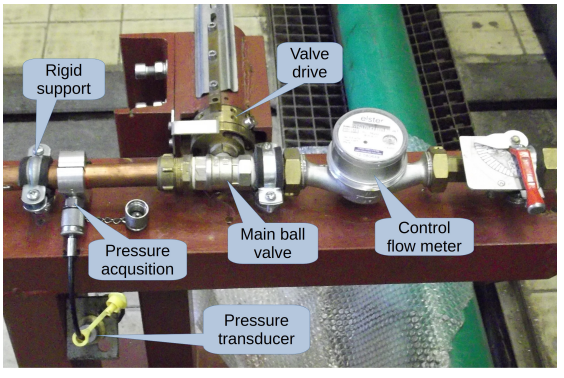

Fig. 4. A view of the pipeline end with shut-off valve, its driving mechanism and pressure acquisition arrangement with an elastic hose (the transducer is invisible).

TABLE 1. Positions of pressure (P) and vibration (D) transducers [13].

Transducer	P1	P2	P3	P4	DA	DB	DC
Position x/L	0.998	0.775	0.574	0.228	0.645	0.316	0.184

3.2. Measurement data for analysis

Many measurements were performed at the laboratory stand. Main investigations were devoted to analysis of WH runs for various elastic supports and initial conditions. Two nominal values of static pressures p_0 were applied – the lower was $p_0 = 0.72\,\mathrm{MPa}$ and the higher one $p_0 = 1.12\,\mathrm{MPa}$ which were denoted correspondingly as "N" and "W". For each of them initial velocities of stationary flow v_0 was varied up to $2.0\,\mathrm{m/s}$. Currently values greater than $v_0 = 0.5\,\mathrm{m/s}$ are of interest because for smaller ones no CS effects were possible. In fact, the limiting value of this velocity was $v_0 = 0.7\,\mathrm{m/s}$ as it is shown in Table 2, where Joukovsky pressure amplitudes Δp are presented for various velocities of an initial flow. These values were calculated with Eq. (1.1), where the wave-speed of the WH wave for the current pipeline, calculated with Eq. (1.2) is $c = 1280\,\mathrm{m/s}$. We can see that for W07 conditions ($p_0 = 1.12\,\mathrm{MPa}$ and $v_0 = 0.7\,\mathrm{m/s}$) there should be no CS effects as $\Delta p < p_0$ but for conditions N07 ($p_0 = 0.72\,\mathrm{MPa}$ and $v_0 = 0.7\,\mathrm{m/s}$) CS effects should happen, similarly as for all higher values of v_0. The strongest effect is expected for conditions N20 ($p_0 = 0.72\,\mathrm{MPa}$, $v_0 = 2.0\,\mathrm{m/s}$). The values of theoretical severity indexes $\tilde{S}$ are also presented in the table. They are calculated with Eq. (2.8) which can be approximated as $\tilde{S} \simeq \Delta p/p_0$, for lower (N) and higher (W) static pressures p_0.

TABLE 2. Pressure amplitudes Δp and theoretical severity indices $\tilde{S}$ for varying velocities v_0.

v_0 [m/s]	0.5	0.7	1.0	1.4	2.0
Δp [MPa]	0.64	0.90	1.28	1.79	2.56
$\tilde{S}_{\mathrm{W}}$	–	–	1.15	1.61	2.31
$\tilde{S}_{\mathrm{N}}$	–	1.25	1.78	2.49	3.56

3.3. Pressure records without column separation

Prior to analysis of CS records some examples of pressures measured along the pipeline for no CS runs are presented and shortly discussed. In Fig. 5 two records, acquired at the valve with the transducer P1 for elastic supports L2, LR and conditions W07 are displayed. No CS effects are observed which is consistent with Table 2. The main WH frequency is about $f_{\mathrm{WH}} = 5.4\,\mathrm{Hz}$ and it is slightly lower for less rigid supports and larger for the most rigid case LR, which must be produced by coupling between pressure oscillations and vibration

of the structure. These results are consistent with the theoretical value which is $f_0 = c/4L \simeq 5.45\,\text{Hz}$, thus the basic WH period is $T_0 = 1/f_0 \simeq 183.5\,\text{ms}$. It can also be noticed that in the L2 record (Fig. 5(a)) the main mode is dominant in comparison with higher components, while for the LR case they must have larger amplitudes which can be concluded from the shape of initial oscillations. Besides, at both runs high frequency (HF) oscillations superimposed on the main WH wave can be noticed at the first few peaks which is the effect of fast valve closure and generation of the transient response of the structure and FSI. They are presented in a zoom-in form by stretching the time axis and presented as details A and B. Their appearance and understanding can be explained with the general form of solutions to the governing equations (2.1) and (2.2) which show the influence of structural vibration on pressures by FSI couplings [12].

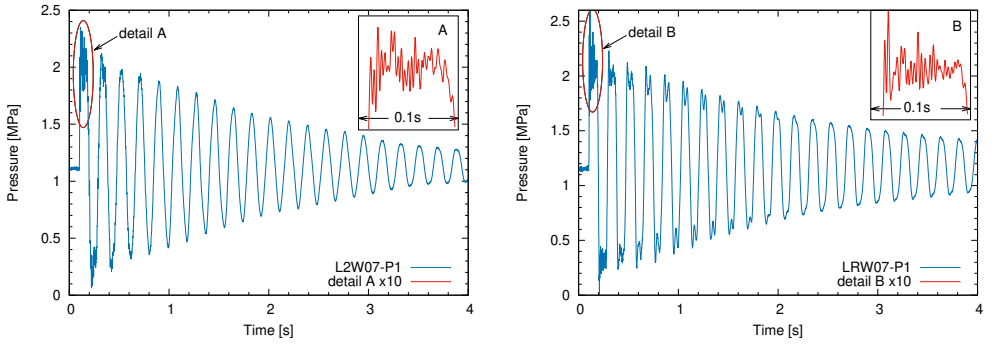

(a) (b)

FIG. 5. Pressures P1 (at the valve) for conditions W07 and supports stiffness L2 or LR. Details A and B show HF oscillations at the first WH peaks stretched in time ten times.

An interesting observation discussed in previous works is that damping of WH pressure amplitudes is stronger for less rigid supports [11, 13, 46]. Average results of logarithmic damping decrements of the main oscillations calculated with different methods for various support configurations were determined as $\delta_{\text{L2}} = 0.096$, $\delta_{\text{L3}} = 0.086$, $\delta_{\text{L4}} = 0.083$, $\delta_{\text{LR}} = 0.070$. In the next Fig. 6 the results of pressure runs at sensors P3 and P4 for the same conditions W07 are presented for L4 supports. A shift of the initial pulse can be observed, which is a result of the time necessary for the wavefront to travel from the valve to each sensor. The HF disturbances are now weaker due to a larger distance from the valve. All the presented plots indicate that WH in the current case is just a kind of standing wave, determined by BC, of an amplitude reduced over time. The results observed at sensor P4 allow to notice how the position influences amplitude changes of various components.

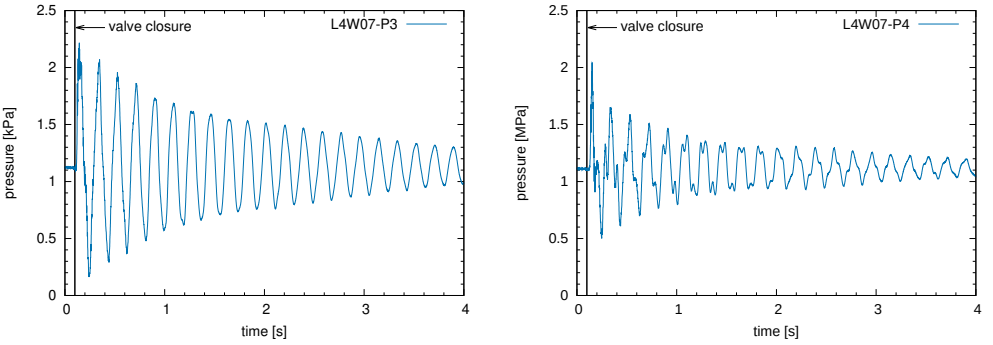

(a) (b)

FIG. 6. Pressures at P3 [13] and P4 sensors for conditions W07 and L4 support configuration.

It can be found that these results differ significantly from the theoretical runs presented in Fig. 1(a), where no dynamic FSI and no liquid – pipe wall friction were assumed. On the other hand, if the influence and modeling of liquid – pipe wall friction without significant FSI is of interest, the analyses and results presented at other works, e.g. [16] can be compared.

4. Measures of column separation severity

4.1. CS severity indices for various supports

In this section CS severity for WH runs is discussed. Severity indexes determined based on the first vapor cavity time duration, given with Eq. (2.7) are used. In Table 3 selected parameters are calculated for various IC and support

TABLE 3. CS severity indexes for various supports and WH strengths.

Nominal v_0	1.0 [m/s]				1.4 [m/s]				2.0 [m/s]				Nominal
Supports	L2	L3	L4	LR	L2	L3	L4	LR	L2	L3	L4	LR	pressure
p_0' [MPa]	1.09	1.09	1.09	1.10	1.05	1.05	1.05	1.07	0.98	0.98	0.99	1.00	
v_0' [m/s]	1.00	0.99	1.01	1.00	1.41	1.39	1.42	1.39	2.05	2.03	1.99	2.02	1.12
T_{cs} [ms]	73	76	81	86	106	107	110	110	156	161	161	170	MPa
S	0.80	0.83	0.88	0.94	1.15	1.17	1.20	1.20	1.70	1.75	1.75	1.85	"W"
β	0.68	0.72	0.75	0.81	0.67	0.69	0.69	0.73	0.63	0.66	0.69	0.72	
p_0' [MPa]	0.69	0.69	0.69	0.71	0.66	0.66	0.66	0.68	0.59	0.58	0.58	0.61	
v_0' [m/s]	1.00	1.00	1.01	1.01	1.40	1.41	1.39	1.43	1.99	2.01	2.00	2.03	0.72
T_{cs} [ms]	115	122	127	129	169	178	181	187	241	252	257	263	MPa
S	1.25	1.33	1.38	1.41	1.84	1.94	1.97	2.04	2.63	2.75	2.80	2.86	"N"
β	0.70	0.72	0.74	0.76	0.68	0.71	0.73	0.76	0.61	0.62	0.64	0.67	

stiffness. As CS effects are expected especially strong at the pipeline end, pressures P1 are analyzed. Besides, detailed values of initial velocities v_0' are presented as they can slightly differ from the nominal ones. The static pressures p_0' at the valve are also presented (rounded into two digits after the coma) as they can be slightly different from the nominal "N" and "W" ones and also they are lower due to friction losses along the pipeline which are larger for higher velocities. Severity indices S were calculated with Eq. (2.7), where $2L/c$ was assumed at $2L/c \simeq 91.8\,\mathrm{ms}$. Due to the earlier introduced definitions (see Section 2.3) we can also determine the dependence between the severity index S and its theoretical value $\tilde{S}$ with the following relation:

$$S = \beta \tilde{S}. \tag{4.1}$$

The coefficients β for each event can be estimated in the following way:

$$\beta = \frac{S}{\tilde{S}} \simeq \frac{S p_0'}{\rho c v_0'} = \frac{p_0' T_{\mathrm{cs}}}{2\rho L v_0'}. \tag{4.2}$$

The main conclusion is that for increased support stiffness, CS effects are getting stronger as their duration times are longer, which is presented in Table 3. However, it must be said that this dependence is not too strong as differences between severity indexes for L2 and LR support configurations are usually of the rank of 10%. These results are illustrated in Fig. 7, where two cases of initial velocity $v_0 = 2\,\mathrm{m/s}$ and lower static pressure "N" are presented – for supports L2 and L4. We can observe the main regularity of longer vapor cavity duration for more rigid supports is valid and it is also maintained for the second CS cycle. The coefficients β indicate the rate of severity index reduction (lower β means smaller S, thus larger reduction). We can observe they (β) are larger for more rigid scenarios and similar for various groups of IC (combinations p_0, v_0) with a slight

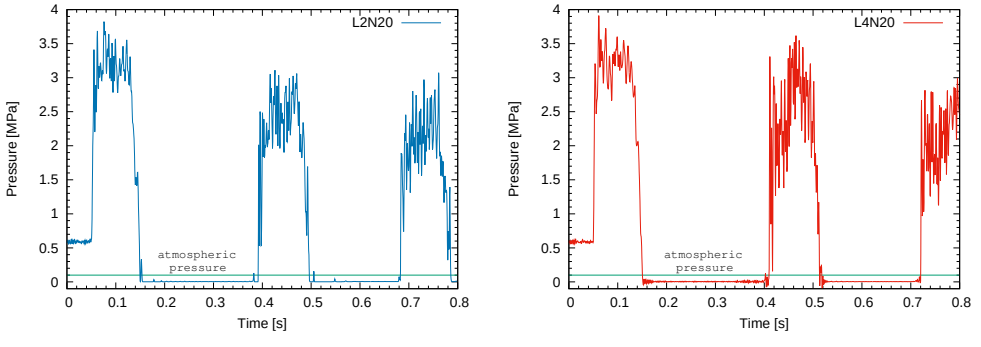

(a) (b)

Fig. 7. WH with CS pressures at P1 for conditions N20 and support configuration L2 or L4.

tendency to be smaller for larger velocity, especially for $v_0 = 2.0\,\mathrm{m/s}$. A specific effect is observed for W10 conditions, where severity indices S are smaller than unity which may seem slightly unusual as we could expect $T_{\mathrm{cs}} \geq 2L/c$. However, in fact the valid dependence is $T_{\mathrm{cs1}} \geq 2L/c$ and currently the theoretical severity indexes are relatively small (conditions W10). Therefore their reduction involved by elastic supports (β coefficients) and FSI may result in $S \leq 1$. This is also an effect produced by changes of the pressure wave shape which is not rectangular as for the theoretical case presented in Fig. 1. Alternatively, we can reduce the influence of the WH waveform shape and estimate the time duration not at the level $p = p_v$ but at $p = p'_0$. Then, severity indices for W10 would be $S_{\mathrm{L2}} = 0.98$, $S_{\mathrm{L3}} = 1.01$, $S_{\mathrm{L4}} = 1.02$, $S_{\mathrm{LR}} = 1.03$.

4.2. Secondary WH actions after collapsing of vapor cavities

Another parameter which may characterize CS severity is the very steep pressure jump after collapsing of vapor cavities. This behavior produces also strong HF FSI effects visible at the pressure peaks as in Fig. 7. We can observe that this effect does not happen for the runs without CS as it is presented in Fig. 5(a), where they exist only at the first peak being a result of fast valve closure within 5 ms. In Fig. 8 these effects are presented explicitly showing two cases of fast (Fig. 8(a)) and slow (Fig. 8(b)) valve closures. The latter was executed just with a human hand which took a time of about 35 ms. We can observe there are no strong HF FSI effects, then. On the other hand, when CS events happen, then HF FSI effects appear for subsequent peaks even if they are not present in the first one. Besides, they are quite strong as the records in Fig. 9 show. Two diagrams are presented of WH runs generated by hand valve closure for lower static pressure N and flows of initial velocities $v_0 = 1.4\,\mathrm{m/s}$ or $v_0 = 2.0\,\mathrm{m/s}$. It is difficult to identify from these diagrams the time of pressure jump after collapse

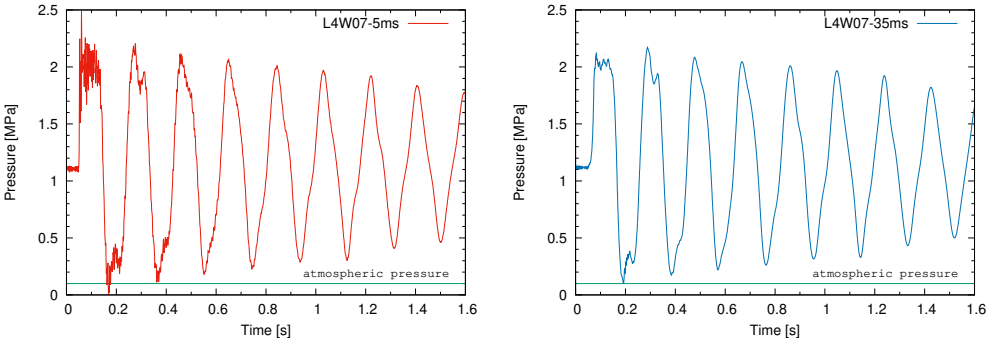

FIG. 8. WH runs for BC L4-W07 produced by (a) fast (5 ms), (b) slow (35 ms) valve closure.

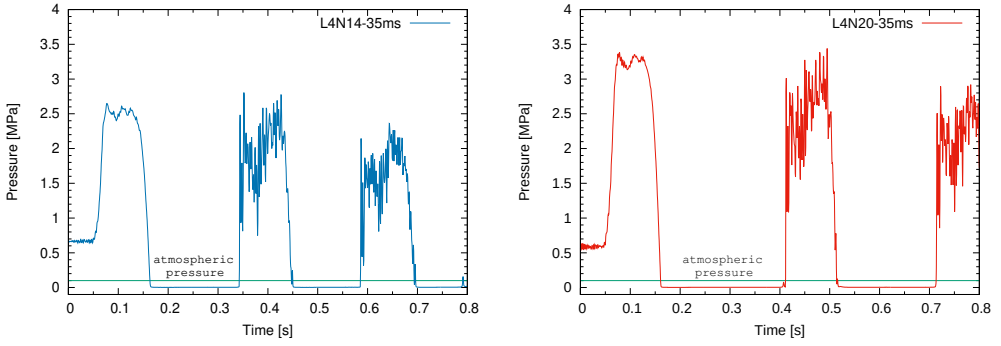

(a) (b)

FIG. 9. WH runs for L4 BC, $p_0 = 0.72\,\mathrm{MPa}$ and time duration of valve closure 35 ms: (a) $v_0 = 1.4\,\mathrm{m/s}$, (b) $v_0 = 2.0\,\mathrm{m/s}$.

of the vapor cavity however, this time was determined from numerical data. For the results presented in Fig. 9, it was found that for N20 IC the pressure jump from 8.3 kPa up to 3.0 MPa takes 2 ms while for N14 conditions the time required for the pressure rise from 8.6 kPa up to 2.5 MPa is 2.5 ms. We can see it is much faster than the time of valve closure. In fact, the times of pressure rise can be expected to be dependent on initial velocities of water column, being shorter when this velocity is larger, as the collision of water columns should be more rapid then. However, a more detailed analysis shows, that this conclusion should be verified, therefore more results were analyzed based on 10 kHz sampled data. It was found that the times of initial pressure rise at the secondary WH events were usually within $1.6 \div 2.4$ ms and no evident regularity was found for the analyzed records. Therefore, the observed pressure response must be a combined effect of steep pulse produced by water column collision and the HF structural response with FSI.

4.3. Energy dissipation produced by column separation effects

Energy dissipation appearing due to CS phenomena can also be a specific measure of their severity as this energy must involve certain outcomes. Some amount of losses are surely transferred into heat within irreversible thermodynamic phase transitions which happens during creation and collapsing of vapor bubbles, but also within complex friction processes in the vapor-liquid mixture. Additional dissipation appears surely in mechanical processes associated with generation of sounds and vibration of the structure. This dissipated energy can be determined by analysis and comparison of pressure amplitudes for various runs at a certain time moment t_0 measured from the beginning of a WH event (pressures at the valve are considered). For the current analysis this time is se-

lected at $t_0 = 3.8\,\mathrm{s}$ and it is marked with a yellow vertical line at $t = 4\,\mathrm{s}$ at the diagrams in Fig. 10. The total initial energy of the system is mainly a kinetic energy of flowing water before closure of the valve, so it can be assumed to be proportional to v_0^2. Some input to this energy also comes from its other forms (mainly elastic potential energy of the supports) thus, the coefficients of proportionality can be slightly higher than M/2, where M is a total mass of water in the pipeline. On the other hand, after valve closure and some additional time required for the transient to be free of CS effects and stable of smoothly lowering amplitudes we can expect this energy to be proportional to p_a^2, where p_a is a current pressure amplitude. This is because the system is linear (when CS is over) and we can assume the energy is parted among its various types (kinetic and elastic potential energy of water and the structure) with similar rates, being proportional to any measure of its response in square. Due to results received in previous works [11, 46] it can be expected that for no CS effects the ratio p_a/v_0 for the same supporting system is approximately the same for various IC, being an effect of calculated logarithmic damping decrements found (see Section 3.3). But if CS behaviors were present, this ratio is expected to be smaller as a fraction of the energy would be lost within effects accompanying the CS phenomenon.

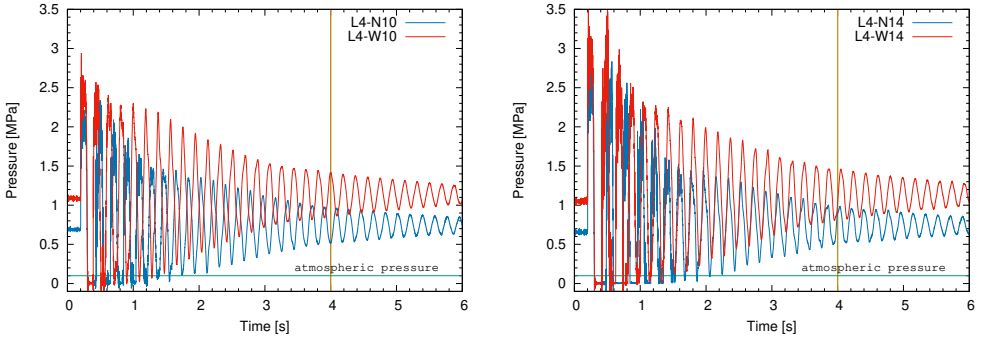

(a) (b)

FIG. 10. WH runs for supports L4 and various initial conditions: (a) N10/W10, (b) N14/W14.

In fact, for further analysis we can use, instead of v_0 the WH pressure p_{WH} corresponding to this value $p_{\mathrm{WH}} = \rho c v_0$. Then, the new ratio $p_a/p_{\mathrm{WH}} = \alpha$ is non-dimensional. However, we have to remember this ratio (its square) does not represent the relation between current and initial energies. This is because, proportionality coefficients are different at the initial and the final state of the system. In Table 4 coefficients $\alpha = p_a/p_{\mathrm{WH}}$ for no CS effects (W05, W07, N05) and their average values $\bar{\alpha}$ for each support type are presented in the first four

Table 4. Amplitude ratios α for WH events of various severity indices.

Supp.	α for no CS effects			$\bar{\alpha}$	α for runs with CS						
syst.	W05	W07	N05	Mean	N20	N14	W20	N10	W14	N07	W10
L2	0.392	0.324	0.426	0.380	0.236	0.216	0.222	0.283	0.286	0.350	0.287
L3	0.429	0.441	0.449	0.440	0.208	0.261	0.267	0.358	0.330	0.429	0.398
L4	0.484	0.485	0.516	0.495	0.259	0.270	0.277	0.348	0.353	0.431	0.436
LR	0.540	0.543	0.520	0.534	0.251	0.268	0.282	0.353	0.338	0.454	0.476
$\tilde{S}$	–	–	–	–	3.56	2.49	2.31	1.78	1.61	1.25	1.15

columns. The results of these ratios for CS runs, i.e. N07, N10, N14, N20, W10, W14, W20 are presented in subsequent columns. They are ordered according to descending values of the theoretical severity index of each run (calculated for nominal pressures and velocities as in Table 2). We can see that all $\alpha = p_a/p_{\mathrm{WH}}$ ratios are lower than the average which is a correct behavior as CS effects produce additional energy losses, thus lower amplitudes. These ratios are also, in general, lower for stronger CS effects as it could be expected. On the other hand, for lower severity indexes they are closer to the mean values without CS. It can also be noticed that for no CS they are similar for various runs and the same support configuration. A bias exists only for the less rigid case L2 – the ratios $\alpha = p_a/p_{\mathrm{WH}}$ for the first three columns are more strongly varied (thus the average can be erroneous). Besides (which is still unexpected), the ratio for N20 is larger than for N14. These effects can be a result of small stiffness of supports FS2 in comparison to the pipeline rigidity, which could produce some non-repeatability or irregular, slow rocking of the pipeline structure in response to WH loads.

5. Additional characteristics of column separation effects

5.1. Shock response spectrum of pressure runs

The shock response spectrum (SRS) method is a technique for severity determination of transients or shock loads in mechanical systems. SRS shows maximal reaction of a simple oscillator exposed to a load, taken versus natural frequency of this oscillator. Usually a small damping ratio is assumed and various responses of the oscillator can be used. The application of this method to WH loads was proposed in [46]. In Fig. 11 two cases of shock spectra of pressure signal are presented for WH runs with and without CS effects. They were received after subtraction of the constant component p_0. By comparing the runs with and without CS effects it can be found that the former are especially stronger for higher frequencies which is the effect of HF disturbances generated with the rapid

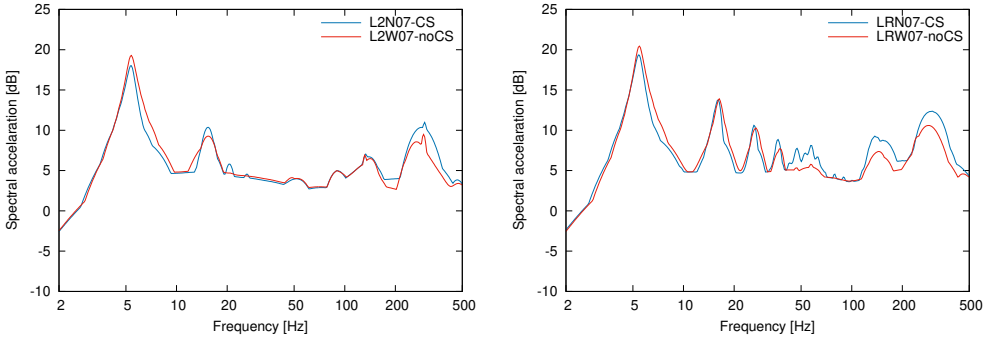

(a) (b)

FIG. 11. Shock response spectra of WH pressures with and without CS effects for various supports: (a) L2; (b) LR.

pressure jump and FSI. However the SRS level for smaller frequencies, especially the main resonance, is slightly lower, which must be an effect of cutting the bottom, CS part of the pressure record. It can also be observed the SRS levels are higher for the more rigid LR case (diagram 11(b) versus 11(a)).

5.2. Pipeline vibration

The severity of WH runs can be also determined based on analyses of pipeline vibration. In Fig. 12 lateral pipeline acceleration at the measuring section DB and supports configuration L4, at $0y$ direction are presented for initial conditions W07 (diagram 12(a)) and N14 (diagram 12(b)) – the latter case has produced CS effects. Vibrations are similar and proportional to initial flow velocities until the first vapor cavity creation and especially its collapse, which is marked at the N14

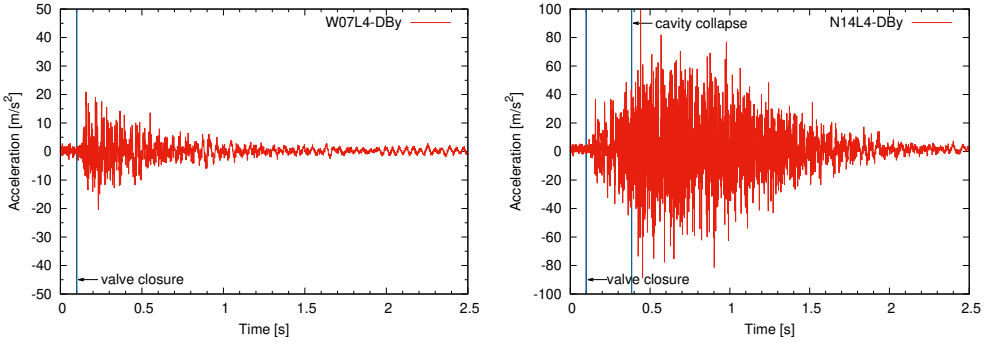

(a) (b)

FIG. 12. Lateral accelerations $0y$ at DB for L4 supports: (a) no CS, W07; (b) CS, N14 IC.

plot with a vertical blue line. Large vibrations are generated then because of the mentioned earlier HF structural vibration produced by the rapid pressure rise. In the next Fig. 13 measured displacements along the pipe axis ($0x$ direction) are presented at the node DC. The vibration at both plots are proportional within the initial time interval, which is physically clear, however, slight asymmetric behavior appears after some time on the CS N14 plot (diagram 13(b)), which is surely produced by the vapor cavity formation. After collapsing of the vapor bubble, stronger vibrations are generated due to a steep pressure rise and FSI. These effects can be also observed in the next Fig. 14 where vibration velocities of the above motion are presented. The plots were received after numerical differentiating of the former ones. One can notice that before vapor cavity formation

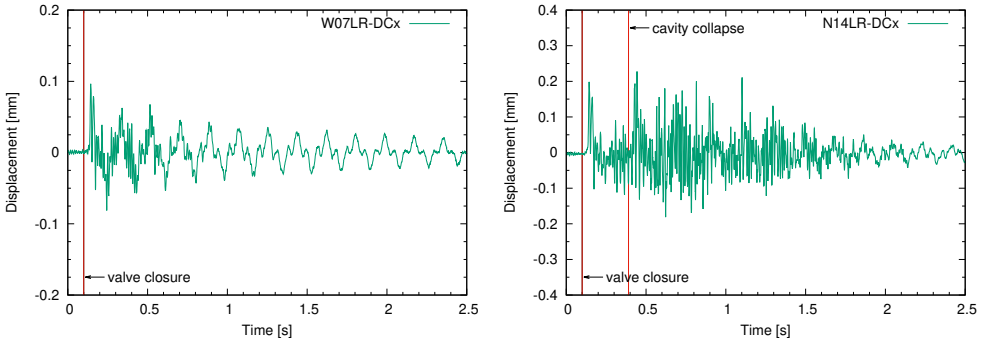

FIG. 13. Longitudinal $0x$ displacement at DC, for LR supports: (a) no CS, W07 IC; (b) CS, N14 IC. The moments of valve closure and cavity collapse are marked with vertical red lines.

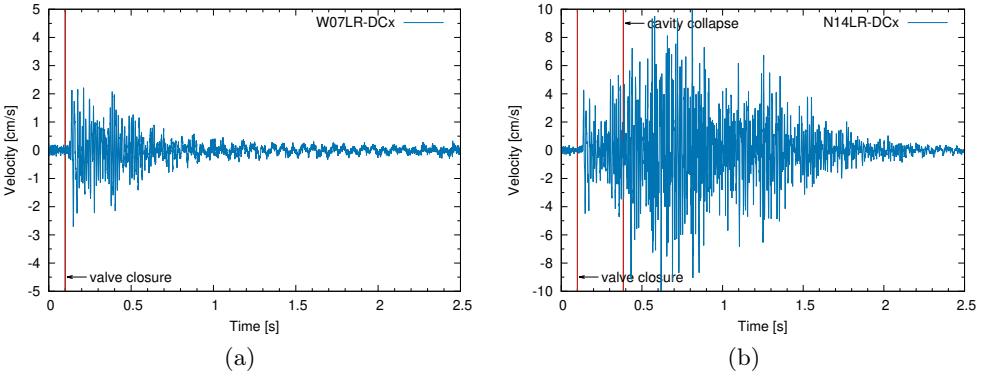

FIG. 14. Longitudinal $0x$ vibration velocities at DC, for LR supports: (a) no CS, W07 IC; (b) CS, N14 IC. The moments of valve closure and cavity collapse are marked with red verticals.

the records are similar and proportional to each other, however, a different pressure course occurs after formation of the vapor cavity and still larger increase in vibration velocities takes place as a result of the cavity collapse.

5.3. Column separation effects at other locations

For the analyses presented in this study pressure records acquired at P1 sensor localized at the pipeline end (close to the valve) were used. This is physically justified as column separation phenomena within such a pipeline structure as well as initial and boundary conditions produce the strongest cavitation and finally CS effects there. However, it can be interesting to compare pressure records measured at various places. In Fig. 15 two pressure runs for IC W20 are presented at P1 and P3 sensors. At sensor P4 (not presented) absolute pressure does not drop below 1 atm and pressure drops at P2 (not shown) are a bit stronger than at P3. One can see typical CS effects are not expected at P3, however, bubbles of vapor are surely created. This conclusion was also acknowledged earlier, for similar experiments performed for a more rigid pipeline [29], where the reader can find photos of various types of cavitation processes – strong CS effects near the valve and individual bubbles at some distant places from the valve.

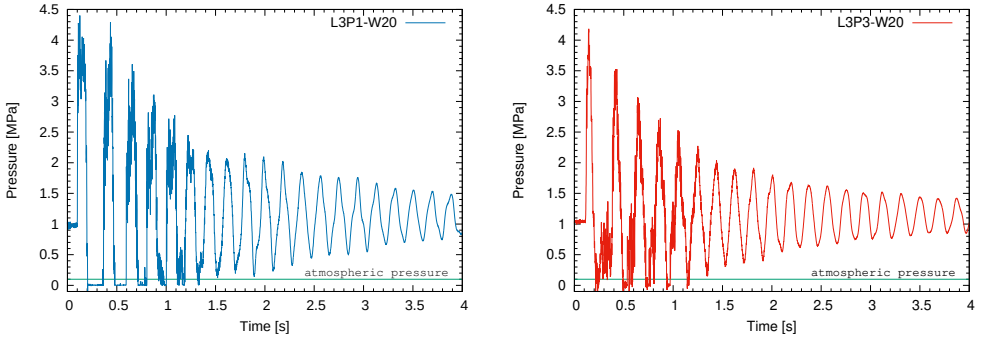

(a) P1 (b) P3

FIG. 15. Pressure runs for L3 support configuration and W20 IC measured at P1 or P3.

6. Conclusions and summary

In the paper analyses of water hammer runs with column separation effects are presented, based on results of experimental measurements conducted in a dedicated, complex, laboratory pipeline compound of several straight pipe reaches joined with knees and fixed to the foundation with elastic supports. This elastic pipeline supporting system was the reason of strong dynamic fluid

structure interaction. Such unique, experimental results constitute a valuable input into systematic research on water hammer phenomena in various scenarios.

An important and valuable conclusion found, is that CS effects were stronger, thus the time duration of the first vapor cavity was longer and the severity index higher, for the pipeline fixed with more rigid supports – this problem and its specific analyses are discussed in Section 4.1. It was also estimated that the energy dissipated within CS events was quite large, and larger for stronger CS effects, thus for higher severity indexes. These losses may have internal origin caused by irreversible thermodynamic phase transitions between liquid and the vapor as well as complex energy dissipation in the viscous flow of vapor-liquid mixture. Another reason could be increased vibration and acoustical effects. The strong pipeline vibration was especially involved due to FSI, after collapsing of vapor cavities and the collision of a water column at the pipeline end. Secondary water hammer events of very steep pressure jumps were produced then, which have involved the strong structural response of higher frequencies and pressure oscillations produced by FSI. A challenge and intention of the author for future research will be to develop models of the WH-FSI phenomenon with CS effects enabling the simulation of the observed behaviors.

Acknowledgments

The results presented in this paper were developed as a part of the IMP PAN statutory research. However, the experimental data used, were acquired within a previous research project (grant N N504 478839) funded by the Ministry of Science and Higher Education of Poland. Thanks are given to other members of the measurement team, as well. Preliminary results of this topic were presented at the 38th Symposium on Hydroacoustics in Hel, Poland, May 6–9, 2025.

References

1. E.B. Wylie, V.L. Streeter, *Fluid Transients in Systems*, 3rd edition, Prentice-Hall, New Jersey, 1993.
2. A. Adamkowski, *Hydraulic Transients in Closed Conduits*, [in Polish, original title: *Przepływy nieustalone cieczy w przewodach zamkniętych*], IMP PAN Publishing House, Maszyny Przepływowe, **34**, Gdansk, 2013.
3. T.C. Lin, G.W. Morgan, *Wave propagation through fluid contained in a cylindrical elastic shell*, Journal of the Acoustical Society of America, **28**, 6, 1165–1173, 1956.
4. D. Wiggert, A. Tijsseling, *Fluid transients and fluid-structure interaction in flexible liquid-filled piping*, Applied Mechanics Review, **54**, 5, 455–481, 2001, https://doi.org/10.1115/1.1404122.
5. S. Henclik, A. Adamkowski, W. Janicki, *Determination of water hammer component frequencies in non-uniform or bifurcated turbine penstock and comparing of analytical*

results with field data, Mechanical Systems and Signal Processing, **228**, 112439, 2025, https://doi.org/10.1016/j.ymssp.2025.112439.

6. C.C. BONIN, *Water-hammer damage to Oigawa power station*, Journal of Engineering for Power T/ASME, **82**, 2, 111–116, 1960, https://doi.org/10.1115/1.3672721.
7. A. ADAMKOWSKI, *Case study: Lapino powerplant penstock failure*, Journal of Hydraulic Engineering, **127**, 7, 547–555, 2001.
8. S. IMIEŁOWSKI, B. ŚNIEGOCKI, *Protection of pipeline bridges against vibrations caused by a water hammer*, Roads and Bridges, **16**, 1, 65–79, 2017, https://doi.org/10.7409/rabdim.017.005.
9. A. TRIKI, M.A. CHAKER, *Compound technique-based inline design strategy for water-hammer control in steel pressurized-piping systems*, International Journal of Pressure Vessels and Piping, **169**, 188–203, 2019, https://doi.org/10.1016/j.ijpvp.2018.12.001.
10. D.C. WIGGERT, F.J. HATFIELD, S. STUCKENBRUCK, *Analysis of liquid and structural transients in piping by the method of characteristics*, Journal of Fluids Engineering T/ASME, **109**, 161–165, 1987.
11. A. ADAMKOWSKI, S. HENCLIK, W. JANICKI, M. LEWANDOWSKI, *The influence of pipeline support stiffness onto the water hammer run*, European Journal of Mechanics — B/Fluids, **61**, Part 2, 297–303, 2017, https://doi.org/10.1016/j.euromechflu.2016.09.010.
12. S. HENCLIK, *Numerical modeling of water hammer with fluid–structure interaction in a pipeline with viscoelastic supports*, Journal of Fluids and Structures, **76**, 469–487, 2018, https://doi.org/10.1016/j.jfluidstructs.2017.10.005.
13. S. HENCLIK, W. JANICKI, *Water hammer runs in elastically supported pipeline and the impact of system vibrations on pressure amplitudes reduction*, International Journal of Engineering Science, **218**, 104400, 2026, https://doi.org/10.1016/j.ijengsci.2025.104400.
14. A. BERGANT, A.R. SIMPSON, J. VITKOVSKY, *Developments in unsteady pipe flow friction modeling*, Journal of Hydraulic Research, **39**, 3, 249–257, 2001.
15. J.P. VITKOVSKY, A. BERGANT, A.R. SIMPSON, M.F. LAMBERT, *Systematic evaluation of one-dimensional unsteady friction models in simple pipelines*, Journal of Hydraulic Engineering, **132**, 7, 696–708, 2006, https://doi.org/10.1061/(ASCE)0733-9429(2006)132:7(696).
16. A. ADAMKOWSKI, M. LEWANDOWSKI, *Experimental examination of unsteady friction models for transient pipe flow simulation*, Journal of Fluids Engineering T/ASME, **128**, 6, 1351–1363, 2006, https://doi.org/10.1115/1.2354521.
17. K. URBANOWICZ, A. BERGANT, M. STOSIAK, M. KARPENKO, M. BOGDEVICIUS, *Developments in analytical wall shear stress modelling for water hammer phenomena*, Journal of Sound and Vibration, **562**, 117848, 2023, https://doi.org/10.1016/j.jsv.2023.117848.
18. R. PUZYREWSKI, J. SAWICKI, *Fundamentals of Fluid Mechanics and Hydraulics*, [in Polish: *Podstawy mechaniki płynów i hydrauliki*], PWN, Warsaw, 1998.
19. A. KERAMAT, A.S. TIJSSELING, Q. HOU, A. AHMADI, *Fluid-structure interaction with pipe-wall viscoelasticity during water hammer*, Journal of Fluids and Structures, **28**, 434–455, 2012, https://doi.org/10.1016/j.jfluidstructs.2011.11.001.
20. A. BAYLE, F. REIN, F. PLOURABOUÉ, *Frequency varying rheology-based fluid-structure-interactions waves in liquid-filled visco-elastic pipes*, Journal of Sound and Vibration, **562**, 117824, 2023, https://doi.org/10.1016/j.jsv.2023.117824.

21. D.D. BUDNY, F.J. HATFIELD, D.C. WIGGERT, *An experimental study on the influence of structural damping on internal fluid pressure during a transient flow*, Journal of Pressure Vessel Technology T/ASME, **112**, 3, 284–290, 1990.

22. G. PEZZINGA, *Unsteady flow in hydraulic networks with polymeric additional pipe*, Journal of Hydraulic Engineering, **128**, 2, 238–244, 2002.

23. S. HENCLIK, *Analytical solution and numerical study on water hammer in a pipeline closed with an elastically attached valve*, Journal of Sound and Vibration, **417**, 245–259, 2018, https://doi.org/10.1016/j.jsv.2017.12.011.

24. R. ZANGANEH, A. AHMADI, A. KERAMAT, *Fluid–structure interaction with viscoelastic supports during waterhammer in a pipeline*, Journal of Fluids and Structures, **54**, 215–234, 2015, https://doi.org/10.1016/j.jfluidstructs.2014.10.016.

25. R.S. HOSSEINI, A. AHMADI, R. ZANGANEH, *Fluid-structure interaction during water hammer in a pipeline with different performance mechanisms of viscoelastic supports*, Journal of Sound and Vibration, **487**, 115527, 2020, https://doi.org/10.1016/j.jsv.2020.115527.

26. M. MITOSEK, *Study of vapor cavitation in series pipe systems*, Journal of Hydraulic Engineering, **126**, 12, 904–911, 2000.

27. A. BERGANT, A.R. SIMPSON, A.S. TIJSSELING, *Water hammer with column separation: A historical review*, Journal of Fluids and Structures, **22**, 2, 135–171, 2006, https://doi.org/10.1016/j.jfluidstructs.2005.08.008.

28. A. BERGANT, A.S. TIJSSELING, J.P. VITKOVSKÝ, A.R. SIMPSON, M.F. LAMBERT, *Discrete vapour cavity model with improved timing of opening and collapse of cavities*, Proceedings of the 2nd IAHR International Meeting – Cavitation and Dynamic Problems in Hydraulic Machinery and Systems, 117–128, Timisoara, Romania, October 24–26, 2007.

29. A. ADAMKOWSKI, M. LEWANDOWSKI, *Investigation of hydraulic transients in a pipeline with column separation*, Journal Hydraulic Engineering, **138**, 11, 935–944, 2012, https://doi.org/10.1061/(ASCE)HY.1943-7900.0000596.

30. A.K. SOARES, D.I.C. COVAS, N.J.G. CARRIÇO, *Transient vaporous cavitation in viscoelastic pipes*, Journal of Hydraulic Research, **50**, 2, 228–235, 2012, https://doi.org/10.1080/00221686.2012.669143.

31. M. SADAFI, A. RIASI, S.A. NOURBAKHSH, *Cavitating flow during water hammer using a generalized interface vaporous cavitation model*, Journal of Fluids and Structures, **34**, 190–201, 2012, https://doi.org/10.1016/j.jfluidstructs.2012.05.014.

32. A.K. SOARES, N.M. MARTINS, D.I.C. COVAS, *Transient vaporous cavitation in a horizontal copper pipe*, Journal of Hydraulic Research, **55**, 5, 731–736, 2017, https://doi.org/10.1080/00221686.2017.1286394.

33. R.E.A. ARNDT, *Cavitation in fluid machinery and hydraulic structures*, Annual Review of Fluid Mechanics, **13**, 273–328, 1981.

34. A.K. KRELLA, *Degradation and protection of materials from cavitation erosion: A review*, Materials, **16**, 5, 2058, 2023, https://doi.org/10.3390/ma16052058.

35. R. AUTRIQUE, E. RODAL, *Experimental verification of steel pipe collapse under vacuum pressure conditions*, Institute of Physics Conference Series: Earth and Environmental Sciences, **49**, 5, 052008, 2016, https://doi.org/10.1088/1755-1315/49/5/052008.

36. D. FAN, A.S. TIJSSELING, *Fluid–structure interaction with cavitation in transient pipe flows*, Journal of Fluids Engineering T/ASME, **114**, 6, 268–274, 1992.

37. A.S. TIJJSELING, A.E. VARDY, D. FAN, *Fluid–structure interaction and transient cavitation in a single-elbow pipe system*, Journal of Fluids and Structures, **10**, 395–420, 1996.

38. A.S. TIJSSELING, A.E. VARDY, *Fluid–structure interaction and transient cavitation tests in a T-piece pipe*, Journal of Fluids and Structures, **20**, 6, 753–762, 2005, https://doi.org/10.1016/j.jfluidstructs.2005.01.003.

39. S.P. TIMOSHENKO, J.M. GERE, *Theory of Elastic Stability*, 2nd edition, Dover, New York, 2009 (republished of 1961 edition from McGraw-Hill Book, New York – London).

40. W. WAN, Y. ZHOU, C. GENG, B. HE, *Numerical modeling of cavity collapse water hammer in pipeline systems: Internal mechanisms and influential factors of transient flow and secondary pressure rise dynamics*, Physics of Fluids, **36**, 087167, 2024, https://doi.org/10.1063/5.0216732.

41. A. ADAMKOWSKI, M. LEWANDOWSKI, *A new method for numerical prediction of liquid column separation accompanying hydraulic transients in pipelines*, Journal of Fluids Engineering T/ASME, **131**, 7, 071302, 2009, https://doi.org/10.1115/1.3153365.

42. Q. SUN, Y. WU, Y. XU, L. CHEN, T.U. JANG, *Coupling quasi-two-dimensional friction model and discrete vapor cavity model for simulation of transient cavitating flows in pipeline systems*, Mathematical Problems in Engineering, **2020**, 8089308, 2020, https://doi.org/10.1155/2020/8089308.

43. C.S. MARTIN, *Experimental investigation of column separation with rapid closure of downstream valve*, Proceedings 4th Int. Conference on Pressure Surges, 77–88, Bath, UK, 1983.

44. A. GRAVELLE, A. ROSS, M.J. PETTIGREW, N.W. MUREITHI, *Damping of tubes due to internal two-phase flow*, Journal of Fluids and Structures, **23**, 3, 447–462, 2007, https://doi.org/10.1016/j.jfluidstructs.2006.09.008.

45. S. HENCLIK, A. MAURIN, *Determination of the stiffness matrix of flat springs for modeling of the boundary condition at a pipeline support*, Mechanical Systems and Signal Processing, **123**, 102–116, 2019, https://doi.org/10.1016/j.ymssp.2018.12.047.

46. S. HENCLIK, *Application of the shock response spectrum method to severity assessment of water hammer loads*, Mechanical Systems and Signal Processing, **157**, 107649, 2021, https://doi.org/10.1016/j.ymssp.2021.107649.

Received July 14, 2025; revised version November 5, 2025.
Published online December 17, 2025.